PHYSICAL REVIEW D 92, 062003 (2015)

Observation of photothermal feedback in a stable dual-carrier optical spring

David Kelley,[1,*] James Lough,[1,2,†] Fabian Mangaña-Sandoval,[1,‡] Antonio Perreca,[1,§] and Stefan W. Ballmer[1,¶]

[1]*Department of Physics, Syracuse University, Syracuse, New York 13244-1130, USA*
[2]*Max-Planck-Institut für Gravitationsphysik (Albert-Einstein-Institut) und Leibniz Universitt, Hannover, Callinstrasse 38, 30167 Hannover, Germany*

(Received 10 July 2015; published 24 September 2015)

We report on the observation of photothermal feedback in a stable dual-carrier optical spring. The optical spring is realized in a 7 cm Fabry-Perot cavity comprised of a suspended 0.4 g small end mirror and a heavy input coupler, illuminated by two optical fields. The frequency, damping, and stability of the optical spring resonance can be tuned by adjusting the power and detuning of the two optical fields, allowing for a precise measurement of the absorption-induced photothermal feedback. The magnitude and frequency dependence of the observed photothermal effect are consistent with predicted corrections due to transverse thermal diffusion and coating structure. While the observed photothermal feedback tends to destabilize the optical spring, we also propose a small coating modification that would change the sign of the effect, making a single-carrier stable optical spring possible.

DOI: 10.1103/PhysRevD.92.062003 PACS numbers: 42.79.Bh, 95.55.Ym, 04.80.Nn, 05.40.Ca

I. INTRODUCTION

The Advanced Laser Interferometer Gravitational-Wave Observatory (Advanced LIGO) [1], together with its international partners Virgo [2] and KAGRA [3], aim to directly observe gravitational waves emitted by astrophysical sources such as the coalescencing of black hole and neutron star binary systems. The installation of the Advanced LIGO detectors is completed, and commissioning towards the first observation run is ongoing. Preliminary astrophysical data is expected in 2015. The sensitivity of those advanced gravitational-wave detectors in the observation band is limited by the quantum noise of light and the thermal noise associated with mirror coatings. A contributor to the thermal noise, expected to dominate in future cryogenic gravitational-wave detectors, is thermo-optic noise [4–6]. It is caused by dissipation through thermal diffusion.

The same physics also leads to an intensity noise coupling, known in the literature as the photothermal effect [7]. The low frequency behavior of the photothermal effect was predicted in [5] and experimentally measured in a Fabry-Perot cavity by De Rosa *et al.* [8]. The physics relevant for the high frequency behavior, dominated by the details of the coating, was investigated in [6] in the context of studying thermo-optic noise. It was extended to a full model of the photothermal transfer function in [9]. Here we explore the thermo-optic effect in the context of an optical spring. The coupling acts as an additional feedback path. The phase of the coupling becomes important and can directly affect the stability of the optical spring resonance. We can exploit this dependence for a precision measurement of the photothermal coupling, even if it is driven by the residual few-ppm absorption of a high-quality optic.

The desire to lower the quantum noise in the gravitational-wave observation band has driven the power circulating in the Advanced LIGO arm cavities up to about 800 kW. The high laser power, in turn, couples the angular suspension modes of the two cavity mirrors. This Sidles-Sigg instability [10] creates a soft (unstable) and a hard mode, whose frequency increases with the intracavity power. The detector's angular control system must control the soft mode and damp the hard mode. At the same time it must not contaminate the observation band, starting at 10 Hz in the case of Advanced LIGO. Future gravitational-wave detectors aim to extend the observational band to even lower frequencies, further aggravating this limitation. We previously proposed a model [11] to overcome the angular instabilities, based on a dual-carrier optical spring scheme demonstrated by Corbitt *et al.*, in 2007 at the LIGO laboratory [12]. The proposed angular trap setup uses two dual-carrier beams to illuminate two suspended optical cavities which share a single end mirror. As a first step towards the experimental demonstration of the scheme we built and operated a prototype, single-cavity optical trap, capable of controlling the cavity length only [13]. The data presented in this paper was taken with this prototype. The next version of the angular trap setup will also allow us to measure the photothermal effect on a folding mirror. Heinert *et al.* [14] predicted excess thermal noise for folding mirrors due to transverse heat diffusion. The result has not yet been experimentally confirmed, but since the same physics will also lead to an enhanced photothermal transfer function, the prediction can be verified with a photothermal transfer function measurement.

*dbkelley@syr.edu
†james.lough@aei.mpg.de
‡fmaganas@syr.edu
§aperreca@ligo.caltech.edu
¶sballmer@syr.edu

The paper is structured as follows: Secs. II and III will review the idea of a dual-carrier optical spring and the photothermal effect respectively. Section IV describes the experimental setup and we discuss the result in Sec. V. Finally, Sec. VI suggests a coating modification to make a stable single-carrier optical spring feasible.

II. DUAL-CARRIER OPTICAL SPRING

A Fabry-Perot cavity detuned from resonance couples the intracavity power linearly to the mirror position. The response is delayed by the cavity storage time. The resulting optical spring constant is given by [11]

$$K_{\mathrm{OS}}^{1\,\mathrm{field}} \approx K_0 \frac{1}{1+\frac{\delta^2}{\gamma^2}-\frac{\Omega^2}{\gamma^2}+i2\frac{\Omega}{\gamma}}, \tag{1}$$

$$K_0 = P_0 t_1^2 r_2^2 \frac{8kr_1r_2}{c(1-r_1r_2)^3}\frac{\frac{\delta}{\gamma}}{(1+\frac{\delta^2}{\gamma^2})}, \tag{2}$$

where P_0 is the incident power, corrected for mode-matching losses, $k=2\pi/\lambda$ is the wave vector of the light, t_i and r_i are the mirror amplitude transmissivity and reflectivity for input coupler ($i=1$) and end mirror ($i=2$), and γ, δ, and Ω are the cavity line, cavity detuning, and mechanical frequency. The value of K_{OS} lies in either the second or the fourth quadrant of the complex plane, and the associated radiation pressure force creates either an antirestoring and damping (red detuning) or a restoring and antidamping force (blue detuning) [15].

Two spatially overlapping optical fields, the carrier and the subcarrier, with opposite detuning sign and with an opportune power ratio can be used to cancel the instability [12]. The total optical spring K_{OS} is the sum of the individual springs

$$K_{\mathrm{OS}} = K_{\mathrm{OS}}^{c} + K_{\mathrm{OS}}^{sc}, \tag{3}$$

where K_{OS}^{c} and K_{OS}^{sc} are given by Eq. (1). The dual-carrier optical spring can be tuned to lie in the first quadrant for the frequency band of interest. When acting on a suspended cavity end mirror with mass m and mechanical suspension spring constant K_m the optical spring becomes a feedback loop with a closed loop response function

$$\frac{x}{F_{\mathrm{ext}}} = \frac{1}{-m\Omega^2 + K_m + K_{\mathrm{OS}}}. \tag{4}$$

The tunability of the optical spring K_{OS} in both magnitude and phase allows experimental fine-tuning of the poles of Eq. (4) to lie exactly on the real axis, resulting in an infinite Q of the optical spring (critical stability). Experimentally this can be done up to a maximum Q, above which the measured transfer function data no longer permits distinguishing between a stable and an unstable spring. The phase of the total spring constant at resonance can then be determined with a precision given by $1/Q$. The suspension mechanical spring constant has to have a positive imaginary part, but it can be designed to be very small. Loss angles of 10^{-5} are easily achievable, and are further diluted by the magnitude of the ratio of K_{OS}/K_m. The contribution to the phase of the total spring constant from the mechanical suspension is thus expected to be negligible. The imaginary part of the optical spring K_{OS} on the other hand is closely related to its real part through Eqs. (3) and (1), and is very accurately predicted based on the resonance frequency, carrier to subcarrier power ratio as well as the detuning of carrier and subcarrier, i.e. only power ratios and frequencies. However, we will see below that the photothermal effect can affect the total transfer function. The first indication of the photothermal effect will be a deviation ϕ in phase from the expectation of Eq. (3) around the optical spring resonance. This is easily and repeatably observable with a precision given by the inverse of the experimentally resolvable Q, and an accuracy determined only by frequency and power ratio measurements. As a function of any such phase deviation ϕ on resonance, the optical spring closed loop response [Eq. (4)] becomes

$$\frac{x}{F_{\mathrm{ext}}} = \frac{1}{-m\Omega^2 + (K_m + K_{\mathrm{OS}})(1+i\phi)}, \tag{5}$$

which on resonance is $\approx [m\Omega_{\mathrm{res}}^2 i(\phi_0+\phi)]^{-1}$. Here ϕ_0 is the known phase of the dual optical spring from Eq. (3) on resonance.

III. PHOTOTHERMAL EFFECT

Power absorption on the surface of an optic leads to an increase of the surface temperature. The depth of the heated layer is given by the diffusion length $d_{\mathrm{diff}} = \sqrt{\kappa/(\rho C\Omega)}$, where κ, C, and ρ are the thermal conductivity, heat capacity, and density of the material, and Ω is the observation angular frequency. In the large-spot size limit, i.e. $\mathrm{w} \gg d_{\mathrm{diff}}$, and neglecting coating effects, the displacement of the surface is given by (e.g. [5,9])

$$\Delta z = \bar{\alpha}\int_0^\infty T dz = \bar{\alpha}\frac{j}{i\Omega\rho C}, \tag{6}$$

where $\bar{\alpha} = 2(1+\sigma)\alpha$ is the effective expansion coefficient under the mechanical constraint that the heated spot is part of a much larger optic [6,16]. α and σ are the regular linear expansion coefficient and the Poisson ratio. $j = P/(\pi \mathrm{w}^2)$ is the absorbed average surface intensity of the Gaussian beam with beam radius w ($1/e^2$ intensity). This simple picture needs two important refinements. First, for frequencies Ω around and below $\Omega_c = 2\kappa/(\rho C \mathrm{w}^2)$ the transverse heat diffusion leads to a multiplicative correction factor to Eq. (6) derived by Cerdonio *et al.* [5]:

$$I(\Omega/\Omega_c) = \frac{1}{\pi}\int_0^\infty du \int_{-\infty}^{\infty} dv \frac{u^2 e^{-u^2/2}}{(u^2+v^2)(1+\frac{(u^2+v^2)}{i\Omega/\Omega_c})}. \quad (7)$$

As expected, for $\Omega \gg \Omega_c$, the correction factor approaches 1. For a fused silica substrate, SiO_2, and a Gaussian beam spot radius of $w = 161\ \mu m$ this correction becomes large below $\Omega_c/(2\pi) = 10$ Hz, but is measurably different from unity even at 1 kHz (see Fig. 1).

Second, for high frequencies, the diffusion length becomes comparable to the coating thickness. Since the optical field is reflected by a dielectric stack, the effective mirror displacement is given by [6,9]

$$_\triangle z = \sum_i \left[\frac{\partial \phi_c}{\partial \phi_i}(\beta_i + \bar{\alpha}_i n_i) + \bar{\alpha}_i\right]\bar{T}_i d_i, \quad (8)$$

where $\bar{\alpha}_i$, $\beta_i = dn/dT$ and n_i are the constrained effective expansion coefficient, the temperature dependence of the index of refraction, and the index of refraction itself for layer i. $\frac{\partial \phi_c}{\partial \phi_i}$, the dependence of the coating reflected phase on the round-trip optical phase in layer i, is always negative, resulting in a sign change and enhancement of the bracket in Eq. (8) for the first few layers. $\bar{T}_i d_i$ is the temperature profile driven by the absorbed intensity j, integrated across layer i. For a $Ta_2O_5:SiO_2$ coating used in gravitational-wave detectors we find a measurable enhancement of the photothermal transfer function around 1 kHz [9]. Additionally, depending on the detailed absorption profile, a sign change can occur above about 100 kHz.

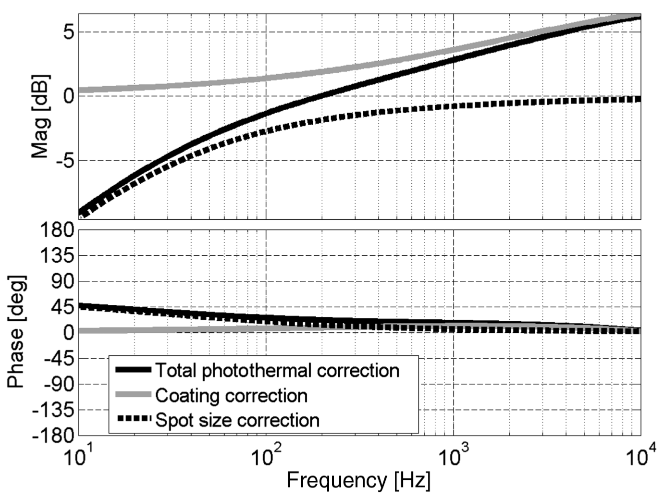

FIG. 1. Correction factors for the photothermal transfer function of a fused silica mirror with a dielectric coating (solid black trace). The solid grey trace is the coating correction for a 13-doublet $\lambda/4$ $Ta_2O_5:SiO_2$ coating. The dashed black trace shows the effect of a Gaussian beam spot with $w = 161\ \mu m$ radius. To get the full transfer function, multiply with Eq. (6), adding an overall $1/f$ shape. The calculation is based on the material parameters shown in Table I.

TABLE I. Parameters for fused silica (SiO_2) and tantulum pentoxide (Ta_2O_5). The values are taken from [6] and [16].

Parameters $Ta_2O_5:SiO_2$	Symbol	SiO_2	Ta_2O_5	Unit
Refractive index (@1064 nm)	n	1.45	2.06	…
Specific heat	C	746	306	J/kg/K
Density	ρ	2200	6850	kg/m^3
Thermal conductivity	κ	1.38	33	W/m/K
Thermal expansion coefficient	α	0.51	3.6	ppm/K
Thermo-optic coefficient (1 μm)	$\beta = \frac{dn}{dT}$	8	14	ppm/K
Poisson ratio	σ	0.17	0.23	…
Youngs modulus	E	72.80	140	GPa

For the experiment parameters discussed in this paper, i.e. a Gaussian beam spot radius of $w = 161\ \mu m$ and a mirror coating with about 13 doublet layers, both effects are relevant in the 100 Hz to 1 kHz band. Their contributions are plotted in Fig. 1.

IV. EXPERIMENTAL SETUP

A. Cavity

The optical spring cavity, described in Table II, is composed of two suspended mirrors in a vacuum chamber, each with radius of curvature ROC = 5 cm and power transmissivity $T = 4.18 \times 10^{-4}$. The measured finesse is 7500 ± 250 and the cavity length is $L_0 = 7.0 \pm 0.2$ cm. We chose a short cavity to minimize frequency noise coupling. The cavity has a free spectral range (FSR) of about 2.14 GHz and cavity pole $f_{\mathrm{pole}} = \gamma/(2\pi) = 143$ kHz. The input mirror mass is 300 g, designed to be heavy to make it insensitive to radiation pressure; it is suspended as a single stage pendulum with mechanical resonances, i.e. position,

TABLE II. Parameters of the optical spring cavity. The range of values for the carrier and subcarrier detuning frequency (δf_C, δf_{SC}) and the input power (P_C, P_{SC}) indicate the variation between individual measurements.

λ_0	1064 nm
Mirror ROC	5.0 cm
L_0	7.0 cm
Spot size	161 μm
FSR	2.14 GHz
Finesse	7500
Cavity pole	143 KHz
δf_C	213–290 KHz
δf_{SC}	27–36 KHz
P_C input	225–239 mW
P_{SC} input	65–78 mW

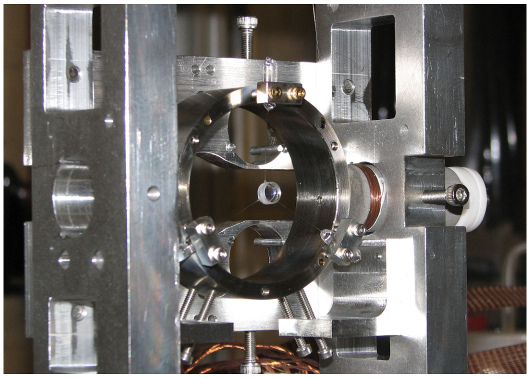

FIG. 2 (color online). A picture of the small end mirror suspended from a steel ring by glass fibers. The ring is suspended from a small optics suspension (SOS) with tungsten wire. The SOS provides dc alignment control while allowing the mirror to move freely above the 18 Hz resonance of the fiber suspension. The end of the fiber is a small glass nub attached to the mirror with epoxy. This produces a fairly high suspension Q of about 5×10^5. The resulting contribution of damping in the optomechanical spring is insignificant compared to the damping from the optical field.

pitch, and yaw, close to 1 Hz. The end mirror has a mass of 0.41 ± 0.01 g and is 7.75 mm in diameter. It is suspended with three glass fibers from a 300 g steel ring, shown in Fig. 2. The steel ring has diameter of 7.6 cm and is itself suspended. The input mirror is actively controlled by an electronic feedback system, while the end mirror is free to move in the glass suspension above its resonance frequency of 18 Hz, and is only subject to the optical spring radiation pressure.

B. Input field preparation

The optical field incident on the optical spring cavity consists of two beams, a carrier and a subcarrier, as described in Sec. II. As shown in Fig. 3, a 1064 nm laser is split into a carrier and a subcarrier beam at the polarizing beam splitter PBS1. In the subcarrier path two acoustic optic modulators (AOMs) are used to impose a relative frequency shift Δ, on the subcarrier beam, leaving it at a set detuning from the carrier beam. Δ is set using an external signal generator (see Sec. IV C). The two beams recombine at PBS2 and proceed towards the Fabry-Perot cavity with opposite polarization. The total power and the power ratio between the carrier and subcarrier beams are set by two half wave plates $\lambda/2$.

The subcarrier beam is modulated by a 35 MHz electro-optic modulator (EOM). We measure the modulated light reflected by the cavity with a resonant radio-frequency photodiode (RFPD) and then demodulate to read-out the cavity length with the Pound-Drever-Hall (PDH) technique [17]. We use the subcarrier to derive a PDH signal because the subcarrier requires less detuning than the carrier. We can use the PDH signal to actuate on the laser and the

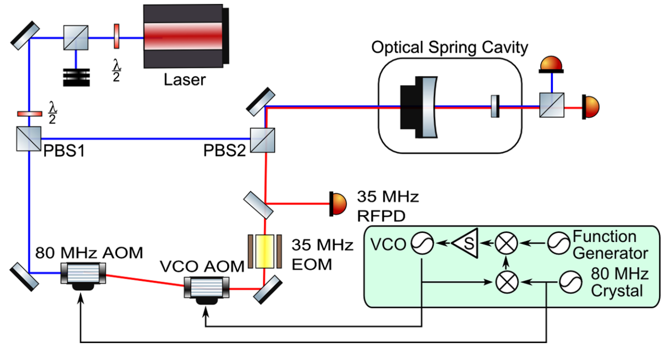

FIG. 3 (color online). A schematic layout of the optical trap experiment. The light from the laser is split into the carrier and subcarrier paths at PBS1, with a ratio determined by the $\lambda/2$ plate. The subcarrier path is frequency shifted by two AOMs under the control of the subcarrier servo (described in detail in Sec. IV C), then recombined with the carrier at PBS2. The coaligned mode-matched beams enter the cavity, then are individually monitored at the output. We can use the 35 MHz EOM and RFPD in a PDH scheme to read-out the cavity length or lock the cavity.

suspensions to lock the cavity, then turn down the gain and use the PDH signal for read-out.

A small offset added to the PDH error signal shifts the locking point of the cavity to the side of the resonance, setting the subcarrier detuning δ_{sc}. We choose to introduce an offset that corresponds to a negative frequency ("red") detuning. Consequently the carrier is positively ("blue") detuned at $\delta_c = \Delta + \delta_{sc}$. An electronic locking servo can be used to process the error signal and feedback to coils, actuating on magnets mounted on the large cavity mirror, and to the laser frequency.

C. Subcarrier servo

The high FSR of our cavity (2.14 GHz) meant that available AOMs, with much lower operating frequency ranges (65–95 MHz), were not suitable to lock the carrier and subcarrier on adjacent resonances. However, this same operating range prevents a single AOM from locking the two beams on the same resonance, due to the small cavity linewidth. Thus, we set the subcarrier on the same resonance fringe as the carrier using two AOMs, each one shifting the laser frequency by about 80 MHz in opposite directions. One is driven by an 80 MHz crystal oscillator, while the other is driven by a servo-locked voltage controlled oscillator (VCO) running slightly offset from 80 MHz (see Fig. 3). To control the offset frequency the 80 MHz signal from the crystal oscillator is mixed with the VCO output, producing a signal at the frequency difference. This difference signal is then mixed with the drive from a function generator, creating the error signal for the servo. The servo drives the frequency modulation input of the VCO, closing the loop and locking the subcarrier beam to a fixed frequency offset from the carrier beam.

This setup significantly suppresses the frequency noise from the VCO. The remaining subcarrier frequency noise (relative to the carrier) is dominated by fluctuations in the path length difference between carrier and subcarrier, see Fig. 3.

V. RESULTS

Using the setup described in the previous section, we locked the cavity using a PDH error signal from the subcarrier, feeding back to the laser frequency actuator and, at low frequencies, the heavy input coupler position. The unity gain frequency was 20 kHz, while the crossover frequency between laser frequency and input coupler position actuation was 250 Hz. In this configuration we fine-tuned the optical spring parameters (carrier and subcarrier offset and power) and measured the PDH control loop open loop transfer function. Dividing out the known PDH loop sensing and actuation function gives us the closed loop transfer functions of the optical springs (Fig. 4). While we demonstrated stable and unstable dual-carrier optical springs, these measurements revealed a significantly smaller phase margin of the optical spring than expected based on Eq. (4), suggesting the presence of a nonradiation-pressure feedback path.

At a few ppm, the absorption A of the mirrors has a very small effect on the cavity finesse and no significant impact on the total transmitted power. However, this small amount of absorption still causes local heating of the optic, driving fluctuations in the surface position of the optic, and thus the cavity length, via the photothermal effect. If this is the dominant effect, we should be able to include the photothermal effect in our model and fit the model to the data, using the absorption as the free parameter. Given a set of optical spring measurements done under similar conditions, we would then expect to find a consistent absorption coefficient across measurements.

A. Analysis

For each measured optical spring transfer function we record the carrier and subcarrier transmitted powers, P_{tc} and P_{ts}, the optical spring resonance frequency f_{res}, and the difference between the carrier and subcarrier detunings $df_c - df_s$, which is set by the function generator frequency.

We can then fit the data d using a model m, which includes the photothermal effect. In particular we fit the ratio d/m using a least-squares fit to minimize E, the error:

$$E = \Sigma \left| \frac{d}{m} - 1 \right|^2. \quad (9)$$

We fit for a small magnitude offset, the subcarrier detuning df_s, and the absorption A. We assess the fitting errors by modeling the noise in each frequency bin of the transfer function measurement, and propagating this noise through the fit. Four of the optical spring transfer functions had a measurement noise of a little less than 1 dB, while the optical springs at 276 and 422 Hz had a significantly higher noise of about 3 dB. We think this noise is dominated by intracavity power fluctuations, most likely due to angular fluctuations.

The remaining parameters (cavity transmitted powers and carrier-subcarrier frequency spacing) we treat as systematic errors. We propagated their measurement errors through the fit. We used a 2% measurement error for the power measurements and a 1 kHz error for the frequency separation.

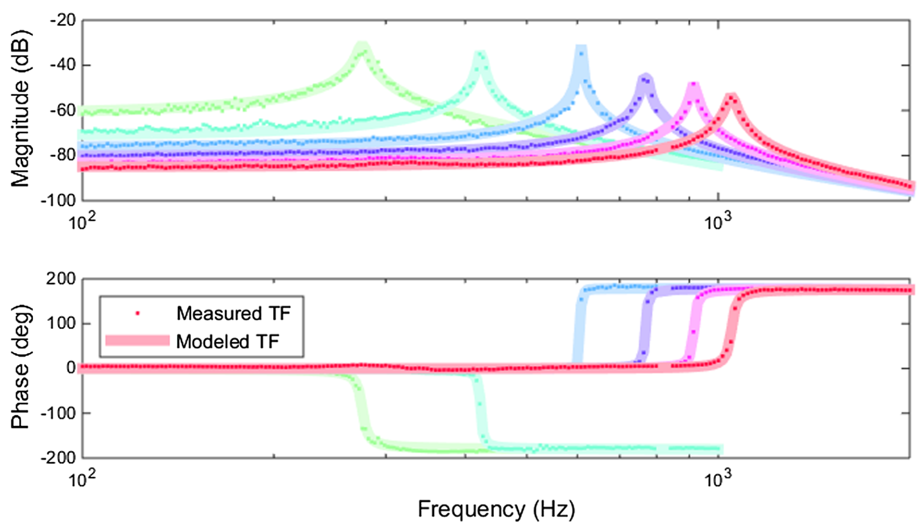

FIG. 4 (color online). Data and modeled transfer function for a series of stable and unstable springs. The modeled transfer functions include the full coating and spot size correction, computed with the measured average absorption. Stable springs show a phase drop of 180° at resonance, while unstable springs show a rise of 180°. The magnitude is given in decibel meter/Newton.

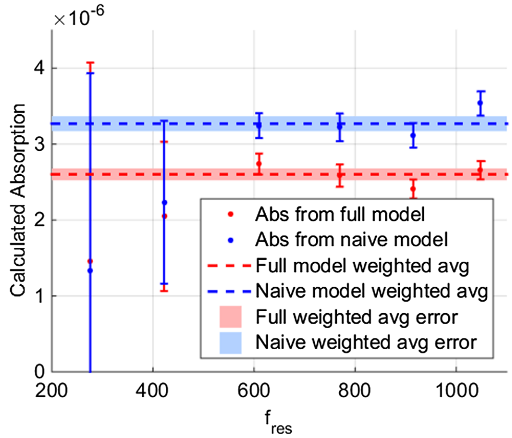

FIG. 5 (color online). Absorption fit for naive and full models. The full model absorption is consistent with a constant absorption of 2.60 ± 0.08 ppm. The naive $1/f$ model predicts $3.27\pm$ 0.10 ppm. The transfer function data for the lowest two resonant frequencies was significantly noisier. Also, at lower frequencies the photothermal effect has a smaller effect on the total optical spring. Both effects result in the larger error bars at low frequencies.

After determining the absorption A for each optical spring transfer function measurement, we can take a statistical-error-weighted average to arrive at the most probable absorption coefficient for the mirror. For the full photothermal model we measure a consistent absorption of 2.60 ± 0.08 ppm (± 0.06 ppm statistical, ± 0.05 ppm systematic) (see Fig. 5). The naive $1/f$ model yields an absorption of 3.27 ± 0.10 ppm (± 0.08 ppm statistical, ± 0.06 ppm systematic). The detailed model with coating and spot size corrections is slightly preferred by the data over the naive $1/f$ model, i.e. the result is more consistent with the same absorption at all frequencies. However, the errors in our measurement are too large to make this statement with any significant certainty.

Since this measurement is based on the missing optical spring phase on resonance [see Eq. (5)], we can also express the result as an extra phase. Near the resonance the optical spring constant is close to real, while the photothermal effect is almost purely imaginary. Thus we approximately find for the extra phase ϕ,

$$\phi = 2m\Omega^2 \frac{c}{2} \frac{\bar{\alpha}}{\Omega \rho C w^2 \pi} A I_{\mathrm{corr}} \approx 0.4° \frac{A I_{\mathrm{corr}}}{1\ \mathrm{ppm}} \frac{f}{1\ \mathrm{kHz}}. \tag{10}$$

Here the leading factor of two accounts for the two mirrors, I_{corr} is the real part of the total correction factor plotted in Fig. 1, and we used the material parameters for fused silica (see Table I). Figure 6 shows the measured extra phase at the resonance frequency of the optical spring, together with the prediction from the photothermal feedback with the best-fit absorption. The figure also shows the expected phase due to the dual-carrier optical spring, as well as the total phase of the complete model. Finally it is worth

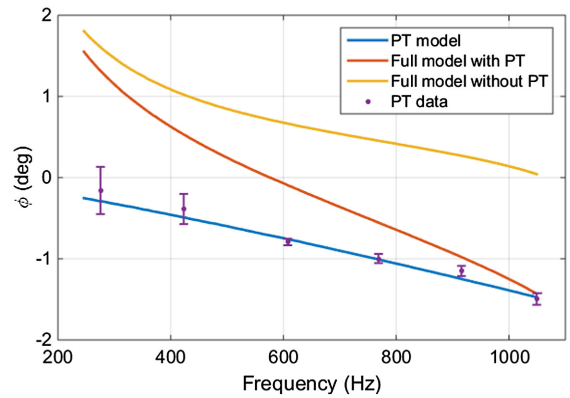

FIG. 6 (color online). Feedback phase at the optical spring resonance frequency due to the optical spring and photothermal (PT) effect. The measured extra phase is consistent with 2.60 ppm of absorption. The error bars are as small as $\pm 0.04°$, a remarkable precision for an open loop transfer function phase measurement.

mentioning that this is a remarkably precise way to measure the phase of the open loop transfer function—the error bars in Fig. 6 are as small as 0.04°. While it is possible to measure the frequency-dependent photothermal phase loss directly in a cavity held on resonance, it would be challenging to achieve the same precision. The magnitude of the effect could be increased using e.g. an external $C0_2$ laser to heat the surface instead of relying on residual absorption, but this would introduce subtle differences due to the different heat deposition depth and uncertainties in the beam overlap between heating and read-out beam.

VI. STABLE SINGLE-CARRIER OPTICAL SPRING

In the experiment at hand the photothermal feedback always pushed the optical spring resonance closer to instability. Perhaps the most interesting question is whether we can change the sign of this feedback path and exploit it to stabilize an otherwise unstable optical spring. It was pointed out in [9] that this naturally occurs above about 100 kHz for a regular dielectric coating. At those frequencies the thermal diffusion length only affects the first few layers of the coating, which affect the overall coating reflected phase differently than the rest of the coating. However, it is actually quite simple to get this sign inversion to occur at a much lower frequency. Increasing the thickness of the initial half-wavelength SiO_2 layer—but keeping it an odd multiple of half the wavelength—will boost the effect from the first layer, thus lowering the frequency at which this sign inversion occurs. Indeed this effect can be strong enough that the damping effect from the subcarrier is not needed to generate a stable optical spring. To illustrate this, Fig. 7 shows a set of six optical springs with parameters identical to the ones shown in Fig. 4, except that we set the subcarrier power to zero (i.e. they are single-carrier optical springs), and we increased the first SiO_2 coating layer from 0.5 to 20.5 wavelength.

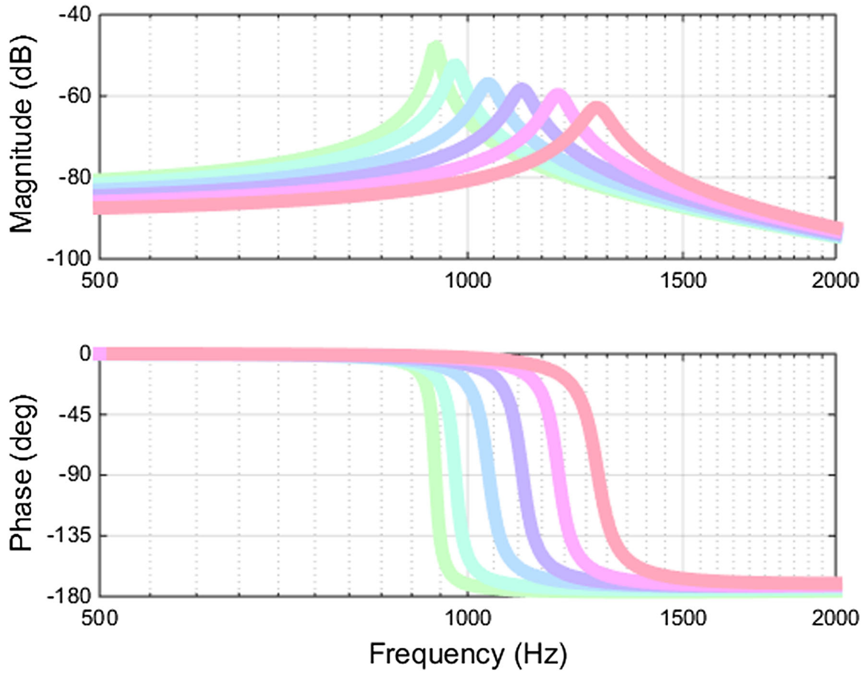

FIG. 7 (color online). Stable single-carrier optical springs (no subcarrier) with modified coating—the first coating layer is 20.5 wavelength thick. See text for details. The six traces otherwise have the same parameters as the best-fit optical springs in Fig. 4. The magnitude is given in decibel meter/Newton.

Such a modified coating would thus allow detuned self-locking of an optical cavity, using just one laser frequency. It does rely on a small amount (order 1 ppm) of optical absorption in the coating, but this level of absorption is often unavoidable anyway, and does not prevent high-finesse cavities.

Due to their intrinsic simplicity stable single-carrier optical springs might open up a number of new applications reaching beyond their use in gravitational-wave detectors. In particular the prospect of tuning feedback in optomechanical applications by designing an appropriate coating is promising and might be useful in a variety of sensor applications. Because stable single-carrier optical springs rely on optical absorption, they will allow vacuum fluctuations to enter the system, particularly at the optical spring resonance frequency. This could in principle constrain their use in quantum-limited systems. However, as in the case of our experiments, in practice the required absorption can be so small that the optical properties of the system are not limited by them.

VII. CONCLUSIONS

We observed photothermal feedback in an experimental optical spring setup for a 0.4 g mirror. We made measurements for a range of optical spring resonant frequencies, and used a least-squares fit to calculate the absorption. The data is consistent with the predictions of the complete model presented in Sec. III, but only slightly prefers it over a simple model that ignores any heat diffusion in the coating and transverse to the optical axis. We also show that a small modification of the first layer of the high-reflectivity coating would be enough to reverse the sign of the photothermal feedback, to the extent that a single-carrier, dynamically and statically stable optical spring becomes feasible.

Repeating the presented measurement with a folding mirror in a cavity should also allow us to confirm the predicted enhancement of thermal noise for folding mirrors [14]. This noise will affect any gravitational-wave interferometer design making use of folding mirrors in the arm cavities [18].

ACKNOWLEDGMENTS

This work was supported by National Science Foundation Grants No. PHY-1068809 and No. PHY-1352511. The authors used computer resources supported by NSF Grants No. PHY-1040231, No. PHY-1104371, and No. PHY-0600953. This document has been assigned LIGO Laboratory Document No. LIGO-P1500003.

[1] G. M. Harry (LIGO Scientific Collaboration), Classical Quantum Gravity **27**, 084006 (2010).
[2] J. Degallaix *et al.*, in *Proceedings of the 9th LISA Symposium, Paris, 2012*, edited by G. Auger, P. Binétruy, and E. Plagnol, Astronomical Society of the Pacific Conference Series Vol. 467 (Astronomical Society of the Pacific, San Francisco, 2013), p. 151.
[3] K. Somiya (KAGRA Collaboration), Classical Quantum Gravity **29**, 124007 (2012).
[4] V. Braginsky, M. Gorodetsky, and S. Vyatchanin, Phys. Lett. A **271**, 303 (2000).
[5] M. Cerdonio, L. Conti, A. Heidmann, and M. Pinard, Phys. Rev. D **63**, 082003 (2001).
[6] M. Evans, S. Ballmer, M. Fejer, P. Fritschel, G. Harry, and G. Ogin, Phys. Rev. D **78**, 102003 (2008).
[7] V. Braginsky, M. Gorodetsky, and S. Vyatchanin, Phys. Lett. A **264**, 1 (1999).
[8] M. De Rosa, L. Conti, M. Cerdonio, M. Pinard, and F. Marin, Phys. Rev. Lett. **89**, 237402 (2002).
[9] S. W. Ballmer, Phys. Rev. D **91**, 023010 (2015).
[10] J. Sidles and D. Sigg, Phys. Lett. A **354**, 167 (2006).
[11] A. Perreca, J. Lough, D. Kelley, and S. W. Ballmer, Phys. Rev. D **89**, 122002 (2014).
[12] T. Corbitt, Y. Chen, E. Innerhofer, H. Müller-Ebhardt, D. Ottaway, H. Rehbein, D. Sigg, S. Whitcomb, C. Wipf, and N. Mavalvala, Phys. Rev. Lett. **98**, 150802 (2007).
[13] J. Lough, Ph.D. thesis, Syracuse University, 2014, http://surface.syr.edu/etd/172.
[14] D. Heinert, K. Craig, H. Grote, S. Hild, H. Lück, R. Nawrodt, D. Simakov, D. V. Vasilyev, S. P. Vyatchanin, and H. Wittel, Phys. Rev. D **90**, 042001 (2014).
[15] B. S. Sheard, M. B. Gray, C. M. Mow-Lowry, D. E. McClelland, and S. E. Whitcomb, Phys. Rev. A **69**, 051801 (2004).
[16] M. M. Fejer, S. Rowan, G. Cagnoli, D. R. M. Crooks, A. Gretarsson, G. M. Harry, J. Hough, S. D. Penn, P. H. Sneddon, and S. P. Vyatchanin, Phys. Rev. D **70**, 082003 (2004).
[17] E. D. Black, Am. J. Phys. **69**, 79 (2001).
[18] S. W. Ballmer and D. J. Ottaway, Phys. Rev. D **88**, 062004 (2013).